Molecular Dynamics Simulation of the Solution Structures of Ha-*ras*-p21 GDP and GTP Complexes: Flexibility, Possible Hinges, and Levers of the Conformational Transition†

José Fernando Díaz, Berthold Wroblowski, and Yves Engelborghs*

Laboratorium voor Chemische and Biologische Dynamica, Katholieke Universiteit Leuven, Celestijnenlaan 200D, B-3001 Leuven, Belgium

Received December 28, 1994; Revised Manuscript Received June 12, 1995®

ABSTRACT: Unconstrained molecular dynamics simulations of the GDP and GTP complexes of Ha-*ras* p21 protein are performed in aqueous environment for 500 ps, using the GROMOS force field. The solvated structures are mutually compared as well as to the X-ray structures [Tong, L. A., de Vos, A. M., Milburn, M. V., & Kim, S. H. (1991) *J. Mol. Biol. 217,* 503−516; Pai, E. F., Krengel, U., Petsko, G. A., Goody, R. S., Kabsh, W., & Wittinghofer, A. (1990) *EMBO J. 9,* 2351−2359]. The simulations show areas of flexibility, with deviations from the original structures. The parts that show differences between the two solvated forms are those from residues 12 to 17, 25 to 38, 41 to 51, 57 to 73, 99 to 112, and 120 to 152, coincident with areas of flexibility. Some of these areas also show differences between the X-ray structures and are part of loops on the surface of the protein. Many of the residues in the ends of these loops undergo dihedral transitions during the solvation process. Of all the dihedral transitions observed, 62% occur around the ends of these loops. This suggests that the ends of the areas from 12 to 17, 25 to 38, and 57 to 73 are the hinge points of the conformational transition between the GTP and the GDP forms. The study of the nucleotide interactions in the solution forms shows that residues 29, 30, and 35 establish contacts with the γ-phosphate and the sugar ring of the GTP and thus these contacts could be proposed as the possible levers of the conformational transition that accompanies GTP hydrolysis.

Ras-p21 proteins, the products of the *ras* onco- and protooncogenes, are guanine binding proteins. The guanine nucleotide binding proteins are involved in the signal transduction process in the cell. They act as molecular switches. In the active state they are bound to guanosine triphosphate (GTP),[1] and in order to switch to the inactive state, the γ-phosphate of the nucleotide has to be hydrolyzed, while the product of this reaction guanosine diphosphate (GDP) remains bound to the protein. Both states show differences in certain areas of the molecule (Tong et al., 1991; Pai et al., 1990) that lead to two different conformational states: the GTP-bound form and the GDP-bound form. In the active conformation these proteins interact with an effector molecule, and the lifetime of the interaction is regulated either by an effector mediation or by the intrinsic GTPase activity of the protein (Kaziro, 1978; Stryer & Bourne, 1986; Gilman, 1987).

The *ras*-p21 proteins are major subjects of biochemical research because approximately 30% of the human tumours contain a point mutation of the *ras* genes. Thus constitute the most prevalent oncogene in human carcinogenesis. They are the products of three highly conserved different genes found in the eukaryotic genome, named Ha(rvey)-, K(irsten)-, and N(euroblastoma)-*ras*. These genes code for 21 kDa proteins that function as molecular switches in signaling events of cell growth and differentiation (Barbacid, 1987; Hall, 1990; Bourne *et al.*, 1991). The *ras*-p21 proteins bind the magnesium complex of guanine nucleotides with high affinity and selectivity (John *et al.*, 1990), and they have a very low intrinsic rate of GTPase activity. This rate can be highly accelerated by the binding of the guanosine triphosphatase activating protein (GAP), which is a ubiquitous protein in higher eukaryotes (Trahey & McCormick, 1987; Adari *et al.*, 1988). The mutations that cause these proteins to be oncogenic are usually found only in a few amino acids of the protein. For example, any amino acid (except proline) that substitutes for glycine in position 12 results in an oncogenic protein (Barbacid, 1987; Seeburg *et al.*, 1984; Pincus *et al.*, 1983). Other positions at which amino acid substitution results in transforming proteins include positions 13, 59, 61, and 63 (Barbacid, 1987). Amino acid Gln61 has been proposed as the general base that catalyzes the γ-phosphate hydrolysis (Langen *et al.*, 1992; Frech *et al.*, 1994). The mutations in amino acids 12 and 13 are located in the first of the 10 loops that connect the five helices and the central six-stranded β-sheet (Figure 1) that constitute the secondary structure of the Ha-*ras*-p21 protein (Wittinghofer & Pai, 1991). These mutations are known for having conformational effects on loop L1 (Brand-Rauf *et al.*, 1988). This loop (L1) is the so-called "phosphate binding loop" or P-loop, and it contains a consensus sequence Gly-X-X-X-X-Gly-Lys that comprises part of a phosphate binding sequence found in purine nucleotide binding sequences (Saraste *et al.*, 1991). Amino acids 59−64 are part of loop

† Financial support from the Research Council of the Katholieke Universiteit is gratefully acknowledged.

* To whom correspondence should be addressed.

® Abstract published in *Advance ACS Abstracts,* August 1, 1995.

[1] Abbreviations: GDP, 5′-guanosine diphosphate; GTP, 5′-guanosine triphosphate; RMSD, root mean square deviation; RMSF, root mean square fluctuation; NMR, nuclear magnetic resonance; SPC, single point charge; DSSP, definition of secondary structure of proteins.

0006-2960/95/0434-12038$09.00/0

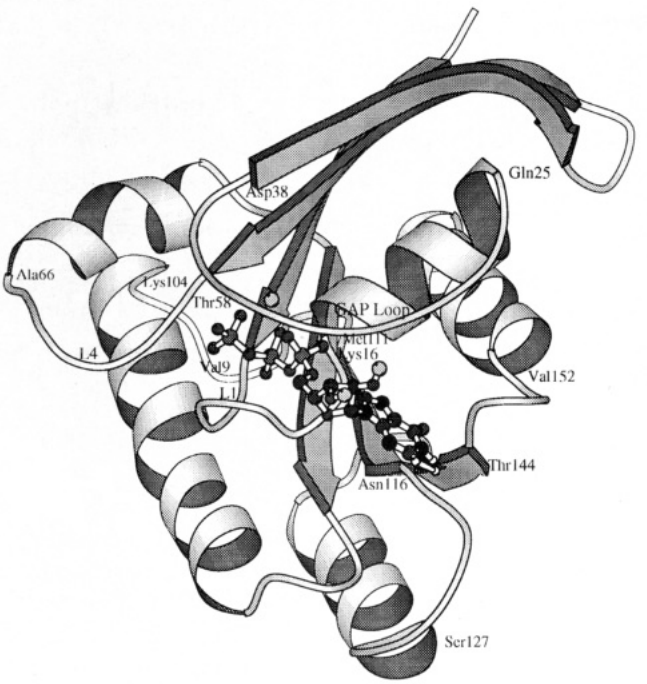

FIGURE 1: Structure of the GTP-Ha-*ras*-p21 protein after 200 ps of MD simulation, showing the areas that undergo conformational changes, the GAP binding loop, the loops 1 and 4, and the secondary structure. This drawing was generated using Molscript (Kraulis, 1991).

4, which is the most preserved part of *ras*-proteins and is also found in all small guanine binding proteins (Valencia *et al.*, 1991).

Until the last two years very little was known about the intracellular signal transduction pathway. The *ras* proteins couple events that occur at the cell surface to changes in gene expression in the nucleus [for a review, see McCormick (1994)]. This is done by transmitting signals from tyrosine kinases to serine−threonine kinases. The signal propagates by the binding of activated tyrosine kinases to adapter molecules via specific SH2−phosphotyrosine interactions. One of these molecules Grb2 is associated with *ras*-GDP/GTP exchange proteins of the Sos class. Binding of Grb2/Sos to membrane-associated tyrosine kinases places the Sos molecule close to the inactive *ras*-GDP molecule, and GDP/GTP exchange occurs. The active *ras*-GTP binds the RAF serine−threonine protein kinase and initiates a kinase cascade that carries signals into the nucleus.

The carcinogenic effect of the majority of *ras* proteins arises from defects in the inactivation system of the *ras*-GTP molecules. It has been shown that the region around 32−45 interacts with the GAP protein (Adari *et al.*, 1988), but the name "effector loop" given to this region is slightly exaggerated because the region that binds the GAP is much larger (Pai *et al.*, 1990). This molecule is a negative regulator of the *ras*-p21 proteins because it binds only to the GTP-form of the protein and accelerates the rate of GTP hydrolysis in the wild-type proteins. The oncogenic proteins are able to bind to the regulatory protein, but this binding does not increase their GTP-ase activity (Adari *et al.*, 1988). Consequently, these molecules are trapped in the active state and constantly transmit the growth signal of the cell. Nevertheless, it should be pointed out that some oncogenic mutants exist that are able to transmit the signal even without any nucleotide bound (Liwo *et al.*, 1994). Other groups of molecules are known to interact with the *ras*-p21 proteins, e.g., nucleotide exchange factors and weak inhibitors of GDP dissociation that should have a control role in the activity of the *ras*-p21 proteins (Wolfman & Macara, 1990).

Up to now two molecular dynamics simulations have been published using the GDP- and GTP-forms of Ha-*ras*-p21 (Dykes *et al.*, 1993; Foley *et al.*, 1992), but, unfortunately, both simulations have been performed using different force fields, the consistent valence force field (CVFF) (Hagler *et al.*, 1985) in the case of the GDP simulation and the AMBER force field (Weiner *et al.*, 1984, 1986) in the case of GTP. The GDP simulation was not based on a real crystallographic structure but on a computer-based model, surrounded by a thin layer of water, whereas the GTP simulation was made using an explicit water box. Therefore, a rigorous comparison of the behavior of both proteins in the simulation could not be done.

Up to now one important attempt has been made to determine crystallographically the pathway of the conformational transition accompanying hydrolysis using time-resolved X-ray crystallography (Schilchting *et al.*, 1990). This study provides some useful information about the structure of the molecule in its GTP state and a direct comparison between the crystallographic structure of the protein in its two states. Unfortunately, the time resolution of the Laue technique used is too low to detect any intermediate that could give any idea about the possible hinges and levers of the conformational transition or about the possible mechanism of triggering.

Another recent paper that also provides an interesting insight in this question is the NMR structure of the GDP form (Kraulis *et al.*, 1994). Unfortunately the NMR structure of a GTP form is not yet available.

In the calculations described here we use the GROMOS force field (van Gunsteren & Berendsen, 1987) to simulate the behavior of the GTP and GDP forms of the Ha-*ras*-p21 in a water- and counterions-containing environment each for a duration of 500 ps, a much longer time than the previous simulations. The goal is to obtain a rigorous comparison of the two solution forms, and to find the flexible areas and conformational differences of the molecule in the two states, and so make a proposal for the possible hinges and levers of the conformational transition and the possible mechanism of triggering. We think that this comparison will provide a better insight in the conformational change that follows nucleotide hydrolysis and leads to the subsequent signal transduction by the *ras*-p21 molecules.

MATERIALS AND METHODS

The starting structures of the GDP form (1Q21) (Tong *et al.*, 1991) and GTP form (P121) (GMPPCP complex) (Pai *et al.*, 1990) of the Ha-*ras*-p21 molecule were obtained from the Brookhaven Protein Data Bank (Birktoft & Blow, 1972).

The GROMOS 87 (van Gunsteren & Berendsen, 1987) package was obtained from Biostructure S. A. (France). The input files for the GROMOS 87 package were mainly generated using the program WHATIF (Vriend, 1990), which was also used for the visualization of the results of the calculations.

The energies of the structures, including the waters identified in the X-ray structures, were first minimized for 100 steps in vacuum using a steepest descent algorithm

(Levitt & Lifson, 1969) and then placed in a truncated octahedral box of SPC water (Berendsen *et al.*, 1981) with the counterions (Cl^- and Na^+), where a minimum distance of 8 Å was kept between the protein and the border of the box. This results in a 68.63 Å wide water box with 4450 water molecules for the GDP form and in a 64.52 Å wide water box with 3550 water molecules for the GTP form. The whole system contains 15 081 or 12 386 atoms for the GDP and GTP cases, respectively. The molecules and the water were again subjected to a steepest descent energy minimization (500 steps). The velocities of the atoms were assigned following a Maxwellian velocity distribution at 100 K. The systems were warmed up in five consecutive steps of 1 ps to 300 K, and a free molecular dynamics simulation was performed for 500 ps using a constant pressure of 1 atm and a constant temperature of 300 K. The temperatures of the protein and the solvent were separately coupled to a water bath (Berendsen et al., 1984) using a coupling constant of 0.1 ps. The pressure was kept constant by coupling to an external pressure bath (Berendsen et al., 1984) with a coupling constant of 0.5 ps. The conditions of the MD simulation were the following: the time step employed was 2 fs, the integration of the equations of motion and energy were done using a leapfrog algorithm included in the GROMOS package, the bond lengths were constrained to equilibrium values using the SHAKE routine (Ryckart *et al.*, 1977; Van Gunsteren & Berensen, 1977), and a cutoff of 8 Å was used for nonbonded interactions (vdW interactions) and of 11 Å for the electrostatic interactions. For analysis the coordinates were saved every 0.1 ps.

The calculations were performed using 4D/210 and Indy Silicon Graphics workstations and DEC Alpha 3000 workstations. The data were analyzed using the programs WHATIF (Vriend, 1990) and SIMLYS (Krüger et al., 1991). For the calculation of the RMSD the structures were fitted using a least-squares fit of the Cα atoms.

RESULTS

Figure 1 shows the α-carbon representation of the GTP-bound form of the Ha-*ras*-p21 after 200 ps of MD simulation. In this representation it can be seen that the three areas (loops L1 and L4 and the GAP-binding loop) in which the oncogenic mutations are located are close to the γ-phosphate of the GTP molecule. Figure 2 shows a plot of the potential energy of the GDP and GTP forms calculated over the 500 ps trajectory and the RMSD from the original structure. As can be seen in both Figure 2 panels A and B, the energy falls rapidly for about 100 ps and then stabilizes. The initial potential energy of the GTP form was $-43\,500$ kJ mol^{-1}, and it drops to a final average value of $-47\,400 \pm 200$ kJ mol^{-1}. The GDP form starts from a higher value of $-40\,800$ kJ mol^{-1} and reaches a final value of $-45\,600 \pm 150$ kJ mol^{-1}. Figure 2 panels C and D show the RMS deviation of the α-carbons during the trajectory. This parameter behaves in a way similar to the energy. The RMSD converges to a mean value of 1.69 Å in the case of the GTP-bound form and 1.86 Å in the case of GDP-bound form [for 1.60 and 2.20 Å in the cases of Foley *et al.* (1992) and Dykes *et al.* (1993)]. The last 350 ps were averaged to generate the final averaged structures.

Comparison of Averaged Structures and Initial Structures. Figure 3 shows the RMSD per residue between the initial

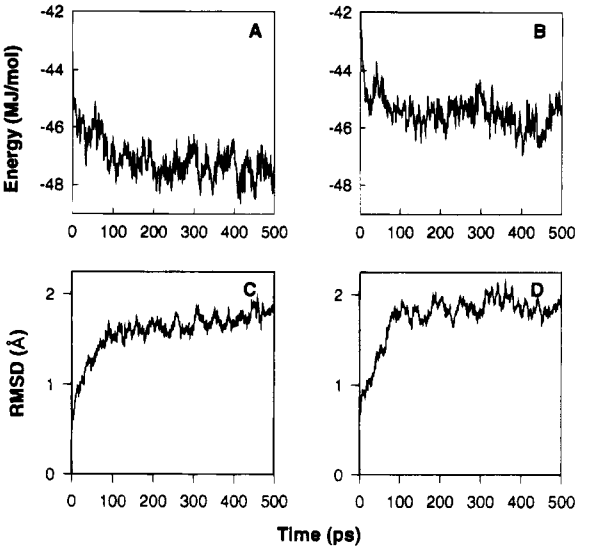

FIGURE 2: Potential energies and RMSD from the X-ray determined structures of the GTP-Ha-*ras*-p21 (A and C) and GDP-Ha-*ras*-p21 (B and D) during the molecular dynamics simulation.

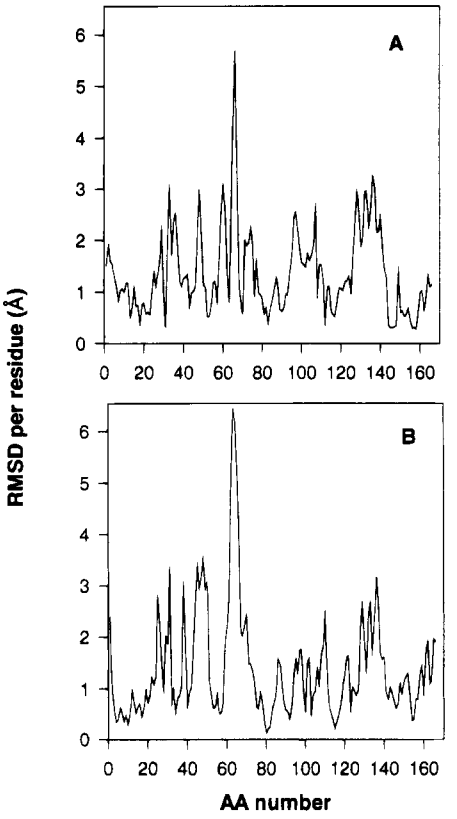

FIGURE 3: RMSD in Å per residue plotted versus the amino acid sequence number between the initial and the averaged solvated forms. (A) GTP-Ha-*ras*-p21 (B) GDP-Ha-*ras*-p21.

structure and the final averaged one. The overall RMS deviations are low: 1.61 Å for the Cα atoms and 2.42 Å for all atoms in the GTP-form and 1.94 Å for the Cα atoms and 2.76 Å for all atoms in the GDP-form. These results indicate that the original structures are not too different from the water equilibrated ones. The deviation of the GDP form from the X-ray structure is larger probably due to the lower resolution of 2.2 Å for the GDP form as compared to 1.54 Å for the GTP form. The areas of deviation are similar in both forms, but not exactly the same. Apart from the deviations in N- and C-terminus which are due to end effects, there are four

Table 1: Secondary Structure of the Ha-*ras*-p21 Proteins as Determined Using the DSSP Algorithm of Kabsch and Sander (1983)

α-helix segments		β-sheet segments	
X-ray GTP form	solution GTP form	X-ray GTP form	solution GTP form
Lys16–Gln25	Lys16–Ile24	Thr2–Gly10	Thr2–Gly10
Ser65–Met72	Arg68–Arg73	Glu37–Ile46	Ser39–Ile46
Thr87–Val103	Thr87–Val103	Glu49–Thr58	Glu49–Thr58
Ser127–Tyr137	Ser127–Tyr137	Gly77–Ala83	Gly77–Ala83
Val152–His166	Val152–His166	Met111–Asn116	Met111–Asn116
X-ray GDP form	solution GDP form	X-ray GDP form	solution GDP form
Lys16–Gln25	Lys16–Ile24	Thr2–Val9	Thr2–Val7
Asp69–Met72	Asp69–Thr74	Asp38–Ile46	Ser39–Ile46
Thr87–Glu91	Thr87–Val103	Glu49–Asp57	Glu49–Leu56
Ile93–Lys104		Gly77–Ala83	Phe78–Ala83
Ser127–Tyr137	Ser127–Tyr137	Met111–Asn116	Val112–Asn116
Val152–His166	Val152–His166	Tyr141–Glu143	Tyr141–Glu143

main areas were residues show large deviation: between the amino acids 20 and 50, 60 and 75, 90 and 110, and 120 and 140. The residues in these areas are also those that show a large flexibility and belong to the more accessible areas (not shown). The areas that show large deviation are in good agreement with those previously reported, for GDP and GTP in the simulations of Dykes *et al.* (1993) and Foley *et al.* (1992). The GDP form shows larger deviations from the original one, especially in the amino acids 62–64, the ones with highest *B* factors, in which the mean deviation is larger than 5 Å.

Secondary Structure Analysis

Table 1 shows the analysis of the secondary structure performed using the Kabsch/Sander DSSP algorithm (Kabsch & Sander, 1983).

GDP form. Fifty-seven amino acids are labeled as helix in the X-ray GDP bound structure and 58 in the GDP bound solvated form, where 55 of them have the same secondary structure definition as in the crystal form. The only differences between the helical structures before and after the solvation are the disruption of the last residue of the first helical segment Gln25 in both nucleotide bound states and the expansion by two residues of the second helical segment. There is a third minor difference consisting in the disappearance of the bending point in the long helical fragment (from Thr87 to Lys104) that exists in the crystal form but not in the solvated form and which has the same structure than the GTP form.

The X-ray and solution forms show larger differences in secondary structure within the β-structure. The X-ray structure of GDP bound Ha-*ras*-p21 has 42 residues in β-sheet conformation, but only 36 of them (all of them having the same definition as in the X-ray form) have the same structure in the solvated form. Some denaturation points appear in the β-sheet parts of the X-ray structure.

First, a shortening occurs in the first segment of β-structure going from Thr2 to Val9 in the X-ray form and from Thr2 to Val7 in the solution form. This denaturation is due to a breaking of the backbone hydrogen bonds of Val8 with Asp57 and Leu79 and of Val9 with Asp80.

Secondly, the Asp38-Asp57 backbone hydrogen bond is lost. Consequently, the only antiparallel sheet in the protein (Asp38–Ile46, Glu49–Asp57) lost two residues, the first and last one. The breaking of these bonds has already been described in the simulation of Foley *et al.* (1992). Also Yamasaki *et al.* (1989) observed a conformational change involving a partial denaturation of the β-sheet around Ser39 and Leu56 in the crystallographic structure of the c-Ha-*ras* gene product when the bound GDP is replaced for GTPγS. This is probably a result of the change in the structure of Thr35 due to the impossibility of hydrogen bonding with a γ-phosphate.

Thirdly, the hydrogen bond Leu6–Gly77 is broken, and so Gly77 loses its β-conformation; the same occurs with the hydrogen bond Phe78–Met111.

Very few intramolecular hydrogen bonds can be found in the GDP-bound structure (Tong et al., 1991). The residues that participate in the intramolecular hydrogen bonds are residues 1, 2, 33, 38, 41, 70, 135, and 165. The residues 33, 38, 41, 70, and 135 lie in the areas 20–50, 60–75, and 120–140 that show large differences in the solvation process. Residue 38 is directly involved in one of the most visible changes involving the loss of two residues in the antiparallel β-sheet (Asp38–Ile46, Glu49–Asp57).

GTP Form. In the GTP-bound form, the implementation of the DSSP algorithm (obtained from EMBL) leads to the identification of 61 amino acids in helix conformation in the X-ray structure and 58 in the solvated form. This can be compared with the simulation of Foley et al. (1992), where respectively, 57 and 61 residues were found. The only differences between the helical structures before and after the solvation are the disruption of the last residue of the first helical segment Gln25, the denaturation of the first three residues of the second helical fragment, and the expansion with one residue at the end of this segment. In the previous simulation by Foley *et al.* (1992) of the GTP form, the main difference found was the expansion with one turn of the second helical fragment, which extends from 68–74 to 65–74. In our study we observed exactly the opposite effect. First, following the EMBL implementation of the DSSP algorithm, these residues are already in helical conformation in the X-ray structure. Secondly, this structure is lost during the solvation process.

Some structural differences could also be found between the β-sheet structures of the GTP forms. The backbone hydrogen bond Asp38–Asp57 and also the Glu37–Thr58 (not present in the GDP forms) are broken, and so the Glu37 and Asp38 loose their β-conformation; but since Asp57 keeps its hydrogen bond with Val8 and Thr58 forms a new hydrogen bond with Val9, the latter keep their β-structure. It could be suggested that the denaturation of the β-sheet structures could arise from any instability due to the force field of GROMOS, but this can be excluded since most of the denaturation points only appear in the solvation process of the X-ray GDP-form (also the one with lower resolution and less crystallographic water).

From the examination of the GTP-bound structure (Pai et al., 1990) intramolecular hydrogen bonding could be found between residues 1, 25, 28, 31, 32, 34, 41, 42, 47, 61, 76, 88, 105, 107, 128, 143, 161, and 166. One of these residues (Gln25) is directly involved in the conformational changes involving the denaturation of the secondary structure. Nevertheless, more of them are in the areas that show large conformational changes in the solvation process, i.e., the N and C termini, the areas between the amino acids 20 and

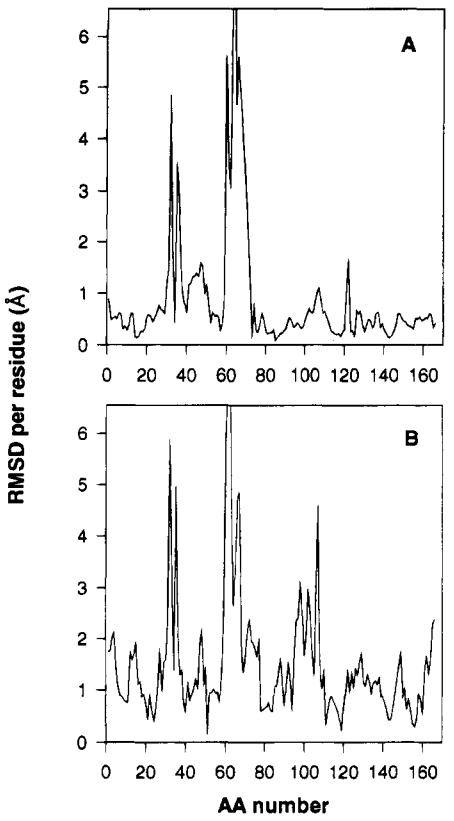

FIGURE 4: RMSD per residue in Å plotted versus the amino acid sequence number between (A) the X-ray determined structures of GTP-Ha-*ras*-p21 and GDP-Ha-*ras*-p21 and (B) the averaged final solvated structures of GTP-Ha-*ras*-p21 and GDP-Ha-*ras*-p21.

50, 60 and 75, 90 and 110, and 120 and 140, and especially the area between the amino acids 20 and 50.

Structural Differences between the GDP and GTP Forms

Figure 4 shows the difference in the position of the residues between the GDP and GTP bound forms of Ha-*ras*-p21 in their crystal (A) and in their solution forms (B). Primarily five areas show differences between the GDP and the GTP forms. The first area comprises residues from Gly12 to Ser17. This part does not show large differences in the crystal form but in the solvated structures. Moreover this loop is more flexible in the GDP form, which is reflected in a larger *B* factor. The second area involves the residues from Gln25 to Asp38. This area shows even larger differences in the solvated form. As has been pointed out before, during the solvation process there is a rearrangement in the hydrogen bonds of the backbone that maintain the structure of the last two residues of this area. The third area which shows smaller conformational differences comprises the residues Arg41−Asp51, which form the loop between both parts of the antiparallel β-sheet from Asp38 to Asp57. Remarkably, the hydrogen bonds between Thr2 and Asp51 are also affected by the solvation process.

The fourth area with large conformational differences comprises the residues from Asp57 to Arg73 in the crystal state and from Asp57 to Gly77 in the solvated state. During the solvation process of the GDP-bound form, the hydrogen bonds between the backbone of Leu6 and Gly77, Asp38 and Asp57, Ala66 and Glu62, Lys5 and Glu 76, and Phe78 and Met111 are broken. Also several hydrogen bonds are broken in this area during the solvation of the GTP-form, the ones between Leu6 and Gly77, Asp38 and Asp57, Glu37 and Thr58, Ala66 and Asp69, Gly75 and Tyr71, Glu76 and Lys5, and Gln99 and Ser65. This is the area that undergoes the largest conformational change and thus should be one of the more flexible areas in solution, so it is logical that so many hydrogen bonds are lost.

The last zone of conformational differences is located from residues Gln99 to Val112. In the crystal form this area has a small RMSD between the GDP-bound and the GTP-bound state, but during the solvation process the deviations are increased and the area with large RMSD between the solvated structures grows to reach the residues Asp85−Val112. This last residue is also involved in the β-sheet denaturation process. There is a sixth area that shows small differences for residues from Leu120 to Val152 but only in the solvated from.

From the point of view of the nucleotide binding area, it could be easily seen in Figure 1 that three of the parts (those from Gly12 to Ser17, Gln25 to Asp38, and Asp57 to Arg 73) with large differences between both conformations are in direct contact with the phosphate region of the nucleotide. These parts together with the segment from Met111 to Asn116 (at the end of another segment that shows conformational differences) form a cup that holds the nucleotide. The three segments are areas without ordered secondary structure around the phosphate of the nucleotides. Thus small differences in the protein nucleotide interactions (see Table 3) that involve the hydrogen bonding of Gly13 and Thr35 with the γ-phosphate, together with the high flexibility of the region Asp57−Arg73 (the one with the highest *B* factor), are responsible for the different conformation necessary for the biological activity of the protein. The differences in the conformation of the area from Asp85 to Val112 can be assigned to the different rearrangement of the different nucleotides in the cup that has an effect in the binding area of the base.

The structures of these areas in the initial and final averaged states are shown in Figure 5A,B. All these areas show positional differences between the GDP and the GTP solvated conformation and are supposed to be involved in the conformational change. They also show differences between the crystal and the solvated states, a large flexibility (see Figures 3, 4, and 6) and a high accessibility to the solvent (not shown).

The parts that show no differences between both structures, from Thr2 to Gly10, from Ala18 to Ile24, from Ser39 to Tyr40, from Leu52 to Leu56, Phe78 to Ile84, and from Leu113 to the end, are all fragments with a well-defined secondary structure as can be seen in Table 1, with a lower flexibility, and all of them are far away from the nucleotide.

Flexible Regions in the Averaged Structures

The RMSF of the GDP and GTP bound forms of Ha-*ras*-p21 in the equilibrated part of the MD (not shown) are in good agreement with the *B* factor of the same amino acids in the crystal form as reported in the two previous simulations (Foley *et al.*, 1992; Dykes *et al.*, 1993). The areas of high flexibility, coincident in both conformations, show the greater differences between the crystal and solvated states and between the GDP-bound and the GTP-bound form. They also show the higher solvent accessibility.

Figure 6 shows the fluctuation of the backbone dihedral angles ϕ and Ψ during the last 350 ps of the simulation of

Table 2: Hydrogen Bonds That Are Lost During the Solvation Process

GDP-Ha-*ras*-p21			GTP-Ha-*ras*-p21		
donor	acceptor	bonded atoms	donor	acceptor	bonded atoms
Lys5	Glu76	N−H OE1[a]	Tyr4	Glu49	OH−HH OE1
Als18	GDP173	N−H O2A	Asp38	Asp57	N−H O
His27	Gln25	ND1−HD1 O[a]	Glu63	Glu63	N−H OE2
Arg41	Asp54	NH2−HH22 OD2	Asp69	Ala66	N−H O
Ala66	Glu62	N−H OE2	Gly75	Tyr71	N−H O
Phe78	Pro110	N−H O	Glu76	Lys5	N−H O
Lys88	Tyr64	NZ−HZ1 OH	Gln99	Ser65	NE2−HE21 O
Glu98	His94	N−H O	Lys101	Glu98	NZ−HZ1 OE2[a]
Gln99	Gln95	N−H O	Arg102	Asp69	NH2−HH21 OD1
Lys101	Glu98	NZ−HZ3 OE2[a]	Asp105	Arg102	N−H O
Asp105	Arg102	N−H O	Ser106	Lys101	N−H O
Ser106	Lys101	N−H O	Arg123	Val125	NH2−HH22 O
Arg123	Glu143	NH1−HH11 OE2	Arg149	Gln22	NH1−HH11 O
Arg123	Val125	NH1−HH12 O	Gln150	Thr148	N−H OG1[a]
Arg123	Glu143	NH2−HH21 OE1	Val152	Arg149	N−H O
Arg123	Glu143	NH2−HH21 OE2	Arg161	Asp47	NH1−HH12 OD1
Arg128	Glu126	NH2−HH22 OE2[a]	Arg164	Glu49	NH1−HH12 OE1
Ile139	Ala134	N−H O			
Arg149	Gln22	NH2−HH22 O			
Gln150	Thr148	N−H OG1			
Val152	Arg149	N−H O			
Arg161	Asp47	NH2−HH22 OD1			
Arg164	Asp47	NH2−HH22 OD2[a]			

[a] Hydrogen bonds that are replaced by another one between the same residues.

Table 3: Nucleotide−Protein Interactions

GDP-Ha-*ras*-p21 (X-ray structure)			GDP-Ha-*ras*-p21 (solvated structure)		
donor	acceptor	bonded atoms	donor	acceptor	bonded atoms
Gly13	GDP173	N−H O2B	Val14	GDP173	N−H O2A
Gly15	GDP173	N−H O1B	Gly15	GDP173	N−H O2A
Lys16	GDP173	N−H O1B	Lys16	GDP173	N−H O2A
Lys16	GDP173	NZ−HZ3 O1B	Ser17	GDP173	N−H O1A
Ser17	GDP173	N−H O3B	Ser17	GDP173	OG−HG O1A
Ala18	GDP173	N−H O2A	Lys147	GDP173	N−HO6
Asn116	GDP173	ND2−HD21 N7	GDP173	Asp119	N2−H1N2 OD2
Lys147	GDP173	N−H O6	GDP173	Asp119	N1−H1N1 OD1
GDP173	Asp119	N2−H1N2 OD2			
GDP173	Asp119	N1−H1N1 OD1			

GTP-Ha-*ras*-p21 (X-ray structure)			GTP-Ha-*ras*-p21 (solvated structure)		
donor	acceptor	bonded atoms	donor	acceptor	bonded atoms
Gly15	GTP173	N−H O1B	Gly13	GTP173	N−H−O3C
Lys16	GTP173	N−H O1B	Val14	GTP173	N−H−O2B
Lys16	GTP173	NZ−HZ1 O3C	Gly15	GTP173	N−H−O3A
Lys16	GTP173	NZ−HZ3 O1B	Lys16	GTP173	N−H−O3A
Ser17	GTP173	N−H O2B	Ala18	GTP173	N−H−O1A
Ala18	GTP173	N−H O1A	Thr35	GTP173	N−H−O3C
Thr35	GTP173	N−H O2C	Thr35	GTP173	OG1−HG1−O2A
Asn116	GTP173	ND2−HD21 N7	Asn116	GTP173	ND2−HD21−N7
GTP173	Asp119	N2−H1N2 OD2	GTP173	Asp119	N2−H1N2−OD2
GTP173	Asp119	N1−H1N1 OD1	GTP173	Asp119	N1−H1N1−OD1
			GTP173	Asp119	N1−H1N1−OD2
			GTP173	Val29	O2*−H1O2*−O
			GTP173	Asp30	O3*−H1O3*−OD1

the solvated GDP and GTP forms. The areas of high backbone dihedral angular fluctuation are the ends of the areas of high positional fluctuation. Table 4 summarizes the dihedral transitions that occur during the last 350 ps of the simulations. Most of these dihedral transitions occur around the ends of the region that undergo conformational transitions. We want to remark that the majority of conformational transitions during the last 350 ps (64% in case of GTP and 61% in case of GDP) occur in the extremes of these areas which are involved in the conformational change between the GTP and the GDP states. Figure 7 is a picture of Ha-*ras*-P21 showing these suspected hinge residues.

Comparison of Intramolecular Hydrogen Bonds and Changes during the Solvation Process

The fact that the solvated structures obtained from the MD simulations are averaged over the 3500 structures that have been stored during the last 350 ps of the trajectory makes it difficult to produce a direct comparison of the hydrogen bonds present in the crystal and in the solvated structures. Since during the averaging process some of the important information could be lost, we calculated the hydrogen bonds

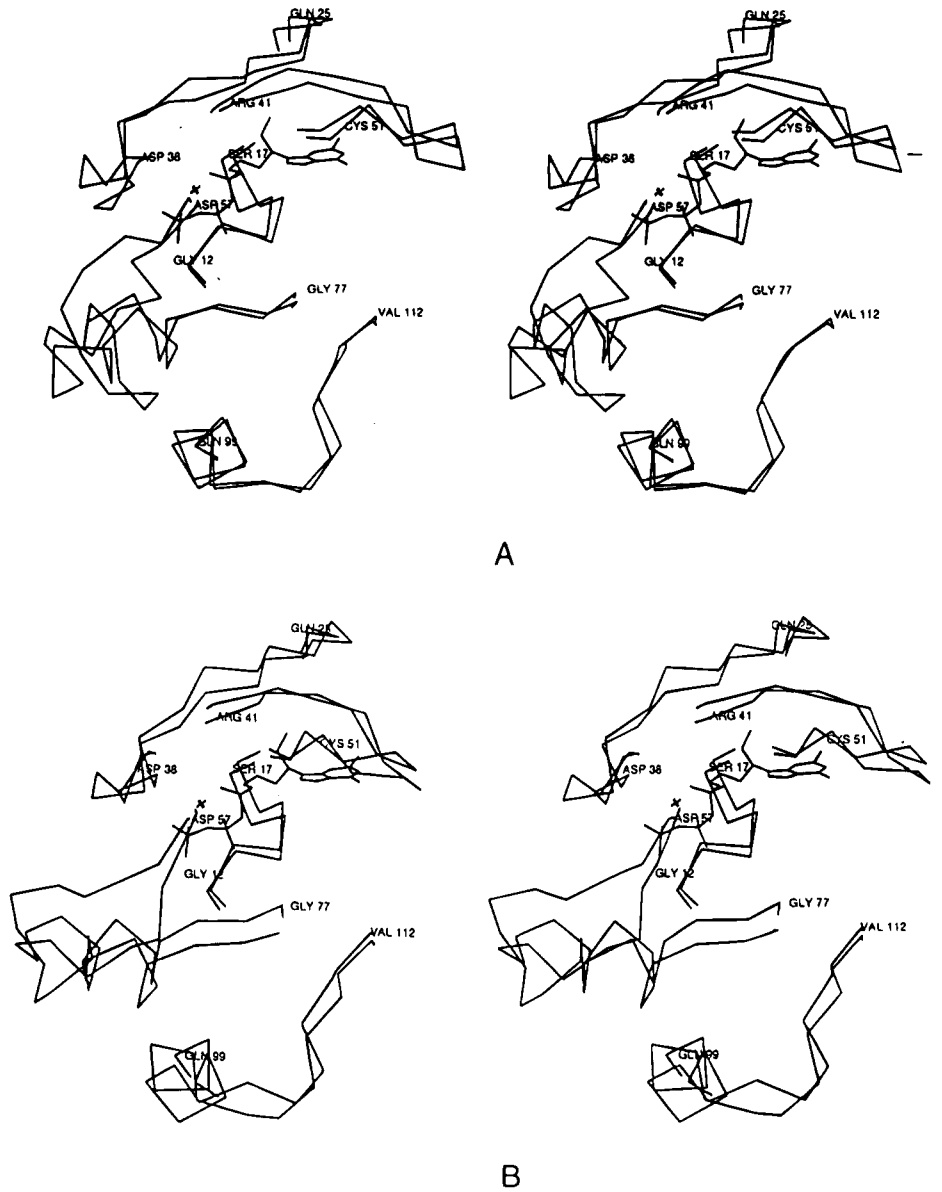

FIGURE 5: Stereoplots of the structures of the areas that shows conformational differences between GTP-Ha-*ras*-p21 and GDP-Ha-*ras*-p21 (A) in the X-ray determined structures and (B) in the averaged solvated structures.

of all structures and their percentage of occurrence. For all the cases a hydrogen bond is considered to be present in the average state when it exists in at least 5% of the structures.

GDP Hydrogen bonds. Table 2 shows the hydrogen bonds present in the crystal forms that are not present in any of the solvated structures. A total of 24 hydrogen bonds present in the GDP bound Ha-*ras*-p21 X-ray determined structure are absent in the MD determined structures. Five of these 24 hydrogen bonds are simply replaced by other hydrogen bonds with the same residue (with a high occurrence), and so their loss does not imply a breakdown of the contacts between these residues. These hydrogen bonds are labeled in Table 2. This leaves 19 intraresidual contacts that are lost during the solvation process. The contacts lost amount to 33 residues. A significant percentage (28%) of these residues (12% of the total) are located at the ends of the areas that undergo conformational changes. Another large percentage of them are inside these areas (52%). Altogether these areas account for nearly 80% of the lost hydrogen bonds, which is not unexpected because they are the areas with larger solvent accessibility and the largest fluctuations.

GTP Hydrogen Bonds. In the solvation process of the GTP form 19 intraresidue hydrogen bonds are lost, two of them being replaced by new internal bonds between the same residues. These changes amount to 25 residues, with 20% of them in the hinge parts and 68% in the areas that undergo conformational changes.

Comparison of the Nucleotide−Protein Interactions in the GDP and the GTP State

The examination of the protein interactions in the four conformations shows that the areas that are binding the nucleotide are quite similar in all conformations. Table 3 shows the hydrogen bond interactions between the Ha-*ras*-p21 polypeptide chain and the nucleotide. Some of the hydrogen bonds are present in all structures. For example, there is one between the side chain of Asp116 and the N7 of the base and from side chain of Asp119 to N1 and N2 of the guanine ring. In all these structures, the residues from Gly13 to Ala18 (the P-loop) are binding the phosphates. The oxygens of the phosphates that are binding the protein vary between the X-ray and the solvated form (since all of them

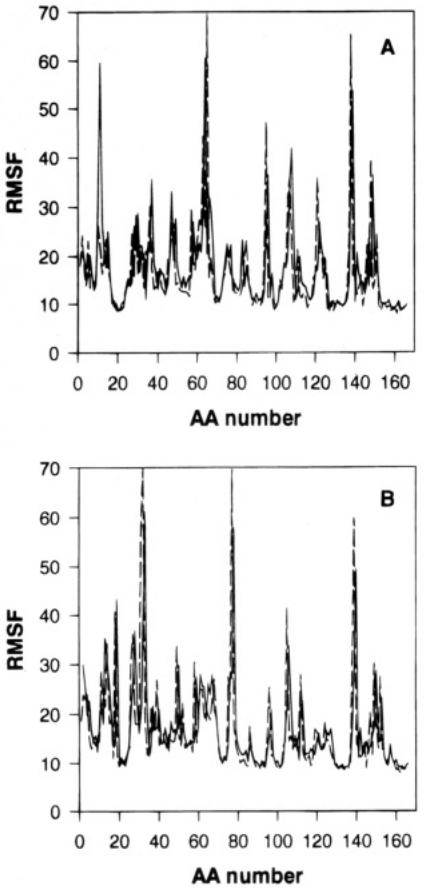

FIGURE 6: RMSF of the ϕ (solid lines) and Ψ (dashed lines) dihedral angles plotted versus the amino acid sequence number, during the last 350 ps of the MD simulation of (A) GTP-Ha-*ras*-p21 and (B) GDP-Ha-*ras*-p21.

Table 4: Amino Acid Bonds That Undergo Conformational Transitions During the Last 350 ps of Simulation

GTP-bound simulation		GDP-bound simulation	
amino acids	number of transitions	amino acids	number of transitions
Val9−Gly10	10	Val9−Gly10	15
Gly10−Ala11	52	Ala11−Gly12	35
Ala11−Gly12	12	Gly12−Gly13	24
Gly12−Gly13	11	Ser17−Ala18	55
Val29−Asp30	19	Gln25−Asn26	8
Tyr32−Asp33	28	Asn26−His27	13
Pro34−Thr35	20	Asp30−Glu31	21
Thr35−Ile36	8	Glu31−Tyr32	63
Ile36−Glu37	66	Thr35−Ile36	26
Glu37−Asp38	8	Glu37−Asp38	5
Tyr40−Arg41	5	Tyr40−Arg41	4
Gly48−Glu49	74	Gly48−Glu49	56
Asp57−Thr58	14	Asp57−Thr58	9
Gly60−Gln61	16	Ala59−Gly60	8
Gln61−Glu62	29	Gly60−Gln61	10
Gly75−Glu76	16	Gln61−Glu62	10
Gln95−Tyr96	11	Gly75−Glu76	68
Asp105−Ser106	14	Lys104−Asp105	29
Asp107−Asp108	20	Cys118−Asp119	10
Ala121−Ala122	7	Tyr137−Gly138	48
Tyr137−Gly138	48	Tyr138−Gly139	42
Thr148−Arg149	46	Thr148−Arg149	30

are equivalent), indicating a certain flexibility of the phosphate chain. The two main differences between the GTP and the GDP forms are the hydrogen bond between the backbone nitrogen of Lys147 and the O6 of the base that are present in the GDP form and not in the GTP form. The

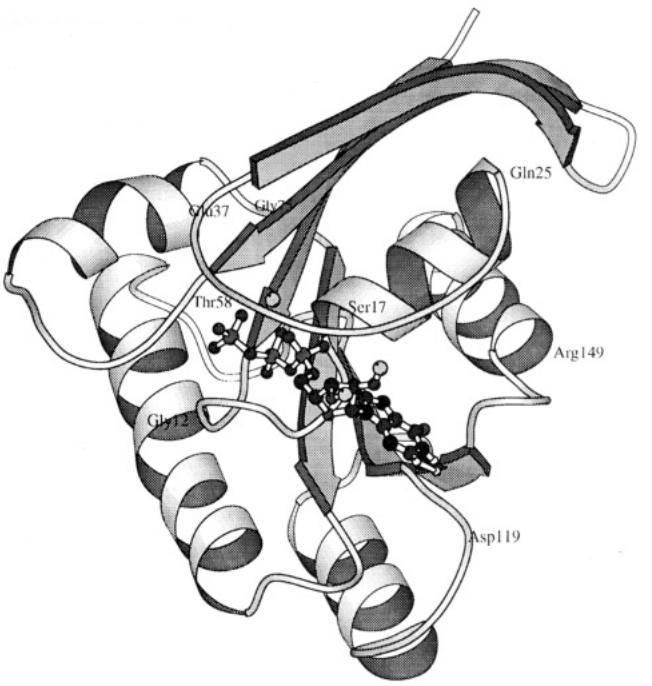

FIGURE 7: Structure of the GTP-Ha-*ras*-p21 protein after 200 ps of MD simulation, showing the hinge and lever residues. This drawing was generated using Molscript (Kraulis, 1991).

other difference occurs in the binding between the region Val29−Thr35 with the triphosphate and the sugar ring.

SUMMARY AND DISCUSSION

We have performed MD calculations of the GDP- and GTP-bound forms of the Ha-*ras*-p21 protein. The purpose was to obtain the solution form of the protein in its two possible states, to explore the conformational space of the protein, and to compare the flexibility areas and the conformational differences between the two states and thus make a prediction of the hinges and levers of the conformational transition between the GDP- and the GTP-bound forms. Since the interactions between the nucleotide and the protein are largely electrostatic and the conformational changes mainly occur in the exposed areas, we used explicit water molecules in the simulation.

It is well known that there are other factors that regulate the function of *ras*-p21 proteins, such as guanosine triphosphatase activating protein (GAP) (Adari *et al.*, 1988) and GTP−GDP exchange proteins of the Sos class (McCormick, 1994). Unfortunately, the structure of their complexes with both, the GTP- and the GDP-bound states of the protein is unknown, and so simulations of the system bound to its different effectors, which probably modify the flexibility of the loops, cannot be done.

We observed conformational differences in certain areas that also show large mobility and flexibility. These areas are those from amino acids 12 to 17, 25 to 38, 41 to 51, 57 to 73, 99 to 112, and 120 to 152. Some of these areas have been identified when the conformational transition has been studied using time-resolved X-ray crystallography (Schlichting *et al.*, 1990).

The parts from 41 to 51, 99 to 112, and 120 to 152 are parts of synthetic peptides, namely, p21 35−47 segment, p21 96−110 segment, and p21 115−126 segment, that act as inhibitors of the *ras* induced oocyte maturation (Dykes *et al.*, 1993). One of the parts (i.e., the one from 99 to 112)

also shows conformational flexibility when it is observed using heteronuclear-edited proton detected NMR (Hu & Redfield, 1993). All these segments could be part of effector domains of the protein since they are able to compete with the intact protein inhibiting the *ras* induced oocyte maturation (Dykes *et al.*, 1993), and so it might be possible that these parts could also adopt multiple conformations (linked to the type of nucleotide bound) in solution. Finally, the recently published NMR solution structure of the GDP-Ha-*ras*-p21 shows that the segments 30−38, 58−66, and 107−109 are mobile on the nanosecond time scale (Kraulis *et al.*, 1994). All those experimental data are consistent with our theoretical study.

The study of the backbone dihedral angular fluctuations in the solvated forms of the molecule during the last 350 ps period shows that all the detected transitions are located inside or close to flexible areas that constitute the phosphate-binding loop, the GAP-binding loop, the catalytic loop, and two areas that are able to inhibit the ras effect (Wittinghofer & Pai, 1991). More importantly, most of these transitions are at the ends of these areas which strongly suggest that these high mobile areas move like rigid bodies around hinge points located at their ends. It can be seen in Figure 7 that the areas delimited by the hinge points 12 and 17, 25 and 38, and 58 to 73 form a kind of cup, rich in charged residues that holds the nucleotide. It is interesting to discuss how the difference in the bound nucleotide affects the flexibility of certain hinge points. The first two hinge points are in the P-loop and so they have different hydrogen bonding in the GDP and the GTP state. Gly13 is directly bound to the oxygen of the γ-phosphate, which results in the absence of dihedral transitions in the bond Gly10−Ala11 in the GDP simulation while 52 transitions are observed in the GTP simulation. The decrease in flexibility in this part of the loop is compensated by an increased flexibility in the Ser17−Ala18 bond that shows 55 transitions in the GDP simulation and none in the GTP-bound. The hinges Gln25−Asn26 and Gly75−Glu76 also show a higher flexibility in the GDP state as a result of the loss of the γ-phosphate. Generally, it can be stated that the nucleotide-binding areas are more flexible in the GDP-bound state, and the presence of the γ-phosphate results in a more rigid conformation.

The experimental data concerning the mutants show that the natural mutants at positions 12, 13, 59, and 61 result in proteins with transforming properties (Barbacid, 1987). All these amino acids are in two of the determined hinge areas, and all of them undergo conformational transitions in this study. The *in vitro* modified residues 60 (Sung et al., 1995), 63 (Fasano et al., 1984), 116 (Walter et al., 1986), and 119 (Sigal et al., 1986) also show transforming properties (63, 116, and 119) or have blocked the conformational transition properties (60). Two of them, 60 and 119, have been identified in this study as highly flexible points; the other two are not exactly in the hinge points but very close to them (63) or are directly involved in the nucleotide binding (119).

Table 5 shows the RMSF of the loops before and after least-squares fit alignment. When the loops of all the structures are superimposed the fluctuation of the positions of the Cα carbons decreases to values around 0.4 Å (a value similar to the one determined for the segment 73−98, which is outside the loops, with or without overimposing) indicating that there are no large differences in the structure of the loops and that the RMSD arises from their positional shifts. In fact, the majority of the transitions that are not located at the ends of these segments are located within either the hyperflexible segment from 57 to 73 [in amino acids (60 and 61) that are quite badly resolved in the X-ray structures] or (48 and 138) in the segments without well known function. That allows us to think that the amino acids 12, 17, 25, 37, 58, 75, 119, and 149 should be the hinges of the conformational change between the GTP and the GDP forms of the Ha-*ras*-p21 protein.

Table 5: RMSF of the Residues in the Areas That Show Conformational Transitions, with and without Alignment, During the Last 350 ps

	GTP-bound simulation		GDP-bound simulation	
segment	RMSF with alignment (Å)	RMSF without alignment (Å)	RMSF with alignment (Å)	RMSF without alignment (Å)
12−17	0.26	0.71	0.21	0.75
25−38	0.45	1.04	0.50	1.06
41−51	0.35	1.10	0.39	1.12
57−73	0.61	1.28	0.78	1.63
73−99	0.35	0.38	0.37	0.41
99−112	0.40	1.11	0.58	1.12
120−152	0.56	1.29	0.52	1.09

Concerning the levers of the conformational change, we have observed that the only differences in the interactions between the protein and the nucleotide are located in one of the effector areas in the so called GAP-binding loop that binds the triphosphate and the sugar ring in the GTP form, or in the amino acid Lys147 whose lateral side chain binds the O6 in the GDP form and not in the GTP form.

We find from the data obtained in this simulation that a plausible hypothesis for the initiation of the conformational change between the GTP and the GDP forms could be the loss of the interactions between the amino acid Thr35 and the γ-phosphate of the nucleotide. This is followed by the movement of the GAP-binding loop as a rigid body. These movements somehow induce the subsequent movement of all the other loops involved in the conformational transition, but the latter will be difficult to observe or to interpret without a pathway simulation.

We will check our hypothesis using techniques for the calculation of pathways of conformational transitions, e.g., the self-penalty method (Elber & Karplus, 1987) and the targeted molecular dynamics method (Schlitter *et al.*, 1994) in order to confirm the sequence of events that triggers the conformational change.

ACKNOWLEDGMENT

We thank the department of theoretical physics of the Katholieke Universiteit Leuven for making available their DEC Alpha 3000 workstations for our MD calculations.

REFERENCES

Adari, H., Lowy, D. R., Willumsen, B. M., Der, C. J., & McCormick, F. (1988) *Science 240*, 518−521.

Barbacid, M. (1987) *Annu. Rev. Biochem. 56*, 779−827.

Berendsen, H. J. C., Postma, J. P. M., Van Gusteren, W. F., & Hermans, J. (1981) in *Intramolecular Forces* (Pullman, B., Ed.) pp 331−342, Reidel, Dordrecht, The Netherlands.

Berendsen, H. J. C., Postma, J. P. M., van Gusteren, W. F., Dinola, A., & Haak, J. R. (1984) *J. Chem. Phys. 81*, 3684−3690.

Birktoft, J. J., & Blow, D. M. (1972) *J. Mol. Biol. 68*, 187−240.

Bourne, H. R., Sanders, D. A., & McCormick, F. (1991) *Nature 349*, 117−126.
Brandt-Rauf, P. W., Carty, R. P., Carucci, J., Avitable, M., Lubowsky, J., & Pincus, M. R. (1988) *J. Protein Chem. 7*, 349−354.
Dykes, D. C., Friedman, F. K., Dykes, S. L., Murphy, R. B., Brand-Rauf, P. W., & Pincus, M. R. (1993) *J. Biomol. Struct. Dyn. 11*, 443−458.
Elber, R., & Karplus, M. (1987) *Chem. Phys. Lett. 139*, 375−380.
Fasano, O., Aldrich, T., Tamanoi, F., Taparowsky, E., Furth, M., & Wigler, M. (1984) *Proc. Natl. Acad. Sci. U.S.A. 81*, 4008−4012.
Foley, C. K., Pedersen, L. G., Charifson, P. S., Darden, T. A., Wittinghofer, A., Pai, E. F., & Anderson, M. W. (1992) *Biochemistry 31*, 4951−4959.
Frech, M., Darden, T. A., Pedersen, L. G., Foley, C. K., Charifson, P. S., Anderrson, M. W., & Wittinghoffer, A. (1994) *Biochemistry 33*, 3237−3244.
Gillman, A. G. (1987) *Annu. Rev. Biochem. 56*, 615−649.
Hagler, A. T., Osgothorpe, D. J., Dauber-Osgothorpe, P., & Hemple, J. C. (1985) *Science 227*, 1309−1315.
Hall, A. (1990) *Science 249*, 635−640.
Hu, J. S., & Redfield, A. G. (1993) *Biochemistry 32*, 6763−6772.
John, J., Sohmen, R. Feuerstein, J., Linke, R. Wittinghofer, A., & Goody, R. S. (1990) *Biochemistry 29*, 6058−6065.
Kabsh, W., & Sander, C. (1983) *Biopolymers 22*, 2577−2637.
Kraulis, P. J. (1991) *J. Appl. Crystallogr. 24*, 946−950.
Kraulis, P. J., Domaille, P. J., Campbell-Burk, S. L., Van Aken, T., & Laue, E. D. (1994) *Biochemistry 33*, 3515−3531.
Kaziro, Y. (1978) *Biochim. Biophys. Acta 505*, 95−127.
Krüger, P., Lüke, M., & Szameit, A. (1991) *Comput. Phys. Commun. 62*, 371−380.
McCormick, F. (1994) *Curr. Opin. Genet. Dev. 4*, 71−76.
Langen, R., Schweins, T., & Warshel, A. (1992) *Biochemistry 31*, 8691−8696.
Levitt, M., & Lifson, S. (1969) *J. Mol. Biol. 46*, 269−279.
Liwo, A., Gibson, K. D., Scheraga, H. A., Brandt-Rauf, R. M., & Pincus, M. R. (1994) *J. Protein Chem. 13*, 237−251.
Pai, E. F., Krengel, U., Petsko, G. A., Goody, R. S., Kabsh, W., & Wittinghofer, A. (1990) *EMBO J. 9*, 2351−2359.
Pincus, M. R., van Renswoode, J., Harford, J. B., Chang, E. H., Carty, R. P., & Klausner, R. D. (1983) *Proc. Natl. Acad. Sci. U.S.A. 80*, 5253−5257.
Ryckaert, J. P., Ciccotti, G., & Berendsen, H. J. C. (1977) *J. Comput. Phys. 23*, 327−341.
Saraste, M., Sibbald, P. R., & Wittinghofer, A. (1991) *Trends Biochem. Sci. 15*, 430−434.
Schlichting, I., Almo, S. C., Rapp, G., Wilson, K., Petratos, K., Lentfer, A., Wittinghofer, A., Kabsh, W., Pai, E. F., Petsko, G. A., & Goody, R. S. (1990) *Nature 345*, 309−315.
Schlitter, J., Engels, M., & Krüger, P. (1994) *J. Mol. Graphics 12*, 84−89.
Seeburg, P. H., Colby, W. W., Capon, D. J., Goeddel, D. V., & Levinson, A. D. (1984) *Nature 312*, 71−75.
Sigal, I. S., Gibbs, J. B., D'Alonzo, J. S., Temeles, G. L., & Wolanski, B. S. (1986) *Proc. Natl. Acad. Sci. U.S.A. 83*, 952−956.
Stryer, L., & Bourne, H. R. (1986) *Annu. Rev. Cell. Biol. 2*, 391−419.
Sung, Y. J., Carter, M., Zhong, J. M., & Hwang, Y. W. (1995) *Biochemistry 34*, 3470−3477.
Tong, L. A., de Vos, A. M., Milburn, M. V., & Kim, S. H. (1991) *J. Mol. Biol. 217*, 503−516.
Trahey, M., & McCormick, F. (1987) *Science 238*, 542−545.
Valencia, A., Chardin, P., Wittinghofer, A., & Sander, C. (1991) *Biochemistry 30*, 4637−4648.
Van Gunsteren, W. F., & Berendsen, H. J. C. (1977) *Mol. Phys. 34*, 1311−1327.
Van Gunsteren, W. F., & Berendsen, H. J. C. (1987) Biomos, Groningen, The Netherlands.
Vriend, G. (1990) *J. Mol. Graphics 8*, 52−56.
Walter, M., Clark, S. G., & Levinson, A. D. (1986) *Science 223*, 649−652.
Weiner, S. J., Kollman, P. A., Case, D. A., Singh, U. C., Chang, C., Alagona, C., Profeta, S., Jr., & Weiner, P. (1984) *J. Am. Chem. Soc. 106*, 765−784.
Weiner, S. J., Kollman, P. A., Nguyen, D. T., & Case, D. A. (1986) *J. Comput. Chem. 7*, 230−252.
Wittinghofer, A., & Pai, E. F. (1991) *Trends Biochem. Sci. 16*, 382−387.
Wolfman, A., & Macara, I. (1990) *Science 248*, 67−69.
Yamasaki, K., Kaway, G., Ito, Y., Muto, Y., Fujita, J., Miyazawa, T., Nishimura, S., & Yokohama (1989) *Biochem. Biophys. Res. Commun. 162*, 1054−1062.

BI942976S